INTL JOURNAL OF ELECTRONICS AND TELECOMMUNICATIONS, 2026, VOL. 72, NO. 3, PP. 1-9
Manuscript received March 13,2026; revised June, 2026. doi: 10.24425/ijet.2026.157927

The influence of bottom slope on sound signals transmission to receiver (Part A) submerged in water column

Roman Salamon, and Jacek Marszal

***Abstract*—Underwater acoustic communications (UAC) in shallow waters is an extremely challenging task. This becomes even more difficult when reliable communication with an object buried in seabed sediments is required. The work presented in two articles (Part A and Part B) is a continuation of the earlier work published in [1]. The articles present the simulation of an acoustic transmission channel, taking into account the bottom slope angle. The simulations utilized the impulse response method and the image source ray tracing technique. The articles present examples of data transmission in a shallow channel with a sloping bottom to a receiver submerged in the water column (Part A) and to a receiver buried in seabed sediments (Part B).**

***Keywords*—underwater acoustic communications; UAC; shallow water channel; multipath propagation; bottom slope**

I. INTRODUCTION

THE Department of Signals and Systems at the Faculty of Electronics, Telecommunications, and Informatics of the Gdańsk University of Technology has been conducting research on underwater wireless communication in shallow waters for many years. This work includes theoretical analyses [1] and tests and measurements in actual field conditions [2-6]. The previous article [1] presented an analysis of acoustic wave propagation conditions in shallow water between a transmitter immersed in the water column and a receiver placed in the water column or buried in bottom sediments. For simplicity, the analysis assumed a constant water depth. In these articles (part A and part B), the presented analysis takes into account the slope of the bottom - rising or falling. In part A, the analysis concerns the transmission of acoustic signals to a receiver placed in the water column, and in part B, to a receiver buried in bottom sediments. Similar to article [1], the analysis was conducted using the image source method [7-9] and impulse response method. This approach to analysing acoustic signal propagation in shallow water differs from that typically presented in the literature, e.g. [10-13]. The use of the impulse response method allows for the analysis of any type of signal and any transmission conditions.

The paper was written as a result of the research project No. DOB-SZAFIR/01/B/017/04/2021 financed by The National Centre for Research and Development of the Republic of Poland.

Authors are with Gdansk University of Technology, Faculty of Electronics, Telecommunications and Informatics, Department of Signals and Systems, Gdańsk, Poland. (e-mail: jacek.marszal@pg.edu.pl).

II. SOUND WAVE PATHS

A simplified model is considered of a water channel with a depth d, in which the water surface and bottom are planes, with the bottom plane inclined at an angle β. A sound signal transmitter is located at a depth of h, and its receiver is located at a distance z from the transmitter, submerged at a depth w, as illustrated in Fig. 1.

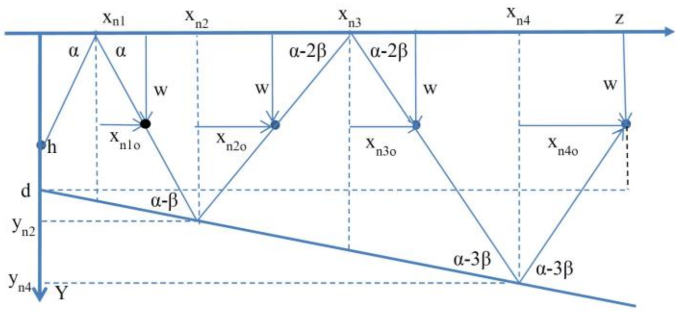

Fig. 1. Sound wave path when reflected first from the water surface.

Fig.1 shows an example of a wave path when the first reflection is from the water surface and the number of reflections n = 4 is even. With an odd number of reflection, the path changes, as can be seen in the figure for three reflections, for example.

For a given number of reflections, there is only one wave path that satisfies Snell's law. Such a path is dependent for each number of reflections n on the channel parameters and the first angle of incidence α_n. The wave path is described explicitly by the coordinates x_{nk} and y_{nk}, where k denotes the number of the consecutive reflection. From the geometric relationships shown in the figure above, these coordinates can be described using the following relationships (Eq. 1-10).

$$x_{n1} = \frac{h}{tg\alpha_n}, \qquad x_{n1o} = \frac{w}{tg\alpha_n}, \qquad y_{n1} = 0 \tag{1}$$

- for odd reflections $k > 1$:

$$x_{nk} = \frac{d + x_{n(k-1)}\{tg[\alpha_n - (k-1)\beta + tg\beta]\}}{tg[\alpha_n - (k-1)\beta]} \tag{2}$$

$$x_{no} = \frac{w}{tg[\alpha_n - (n-1)\beta]} \tag{3}$$

$$y_{nk} = 0 \tag{4}$$

$$y_{no} = w \tag{5}$$

- for even reflections $k > 1$:

$$x_{nk} = \frac{d + x_{n(k-1)} tg[\alpha_n - (k-2)\beta]}{tg[\alpha_n - (k-2)\beta] - tg\beta} \tag{6}$$

$$x_{no} = \frac{d + x_{nk} tg\beta - w}{tg(\alpha_n - n\beta)} \tag{7}$$

$$y_{nk} = 0 \tag{8}$$

$$y_{no} = d + x_{nk} tg\beta - w \tag{9}$$

The initial angle α_n satisfies the Eq. (10):

$$x_{n1} + x_{nn} + x_{no} = z \tag{10}$$

Solving Eq. (10) numerically determines the angles α_n. Note that in order to get correct results, numerical calculations must be performed with a very high degree of accuracy. In the examples shown below, the angles α_n were determined with an accuracy of 0.001 rad. Knowing these angles, the coordinates x_{nk} and y_{nk} for the number of reflections considered are calculated from Eq. (1-10).

Fig. 2-4 show the sound wave paths, the number of which is small, $N = 8$. Calculations were performed for the following parameters: $d = 20$ m, $z = 100$ m, $h = 15$ m, $w = 10$ m. The paths differ in bottom slope angles, as indicated in the figure legends.

The difference in the paths is that in the absence of a slope, the distances of the points x_{nk} and y_{nk} are the same, while with a sloped bottom, they change. With a positive slope angle, they increase with the distance from the transmitter, and with a negative slope angle, they tend to decrease. This results in differences in the arrival of pulse responses, as shown later in this paper.

With a higher number of reflections and greater bottom inclinations, there is an interesting phenomenon of back reflection, as illustrated in Fig. 5-6 and Fig. 7-8. These were obtained for the channel parameters specified above, by varying the bottom slope angles and number of reflections, which is explained in the figure legend.

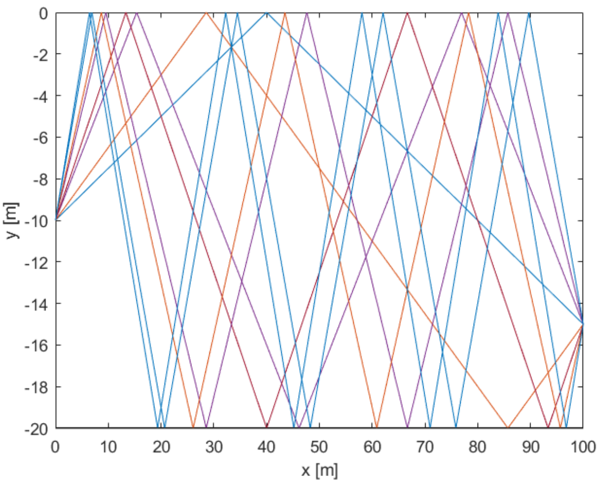

Fig. 2. Sound wave paths for a bottom slope angle $\beta = 0°$.

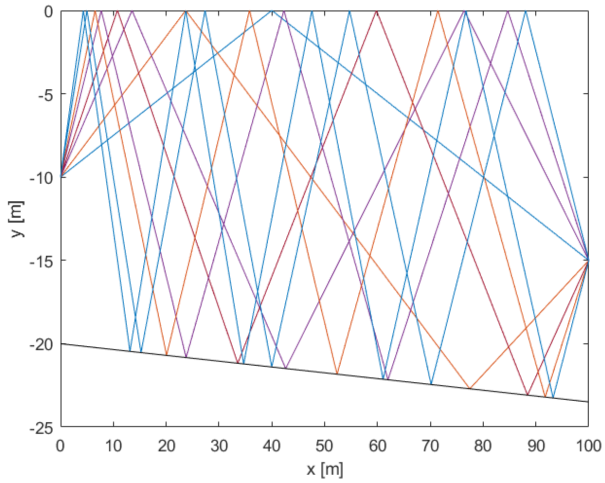

Fig. 3. Sound wave paths for a falling bottom slope angle $\beta = 2°$.

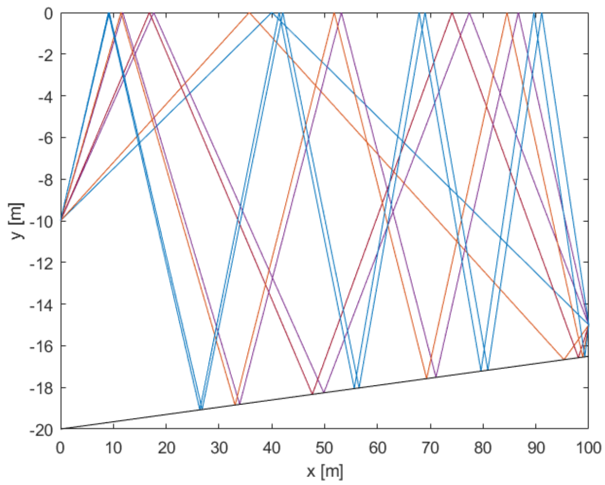

Fig. 4. Sound wave paths for a rising bottom slope angle $\beta = -2°$.

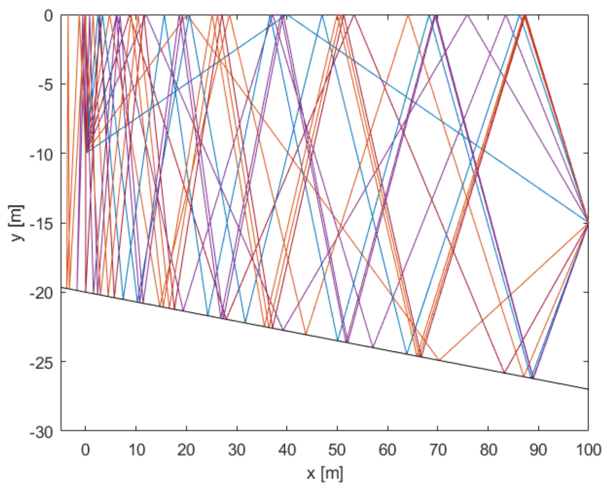

Fig. 5. Sound wave paths for a falling bottom slope angle $\beta = 4°$.

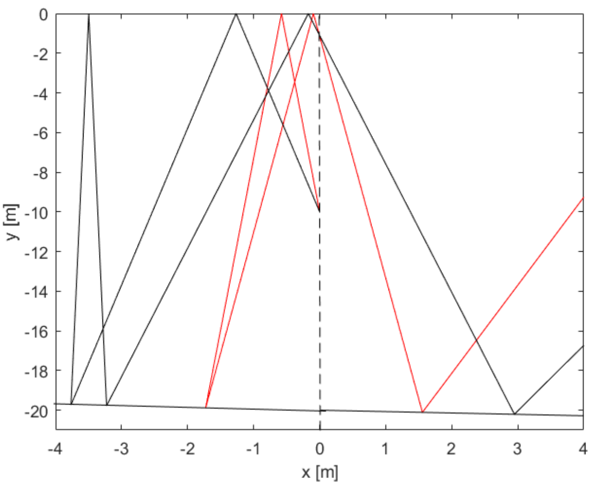

Fig. 6. Enlarged left section of Fig. 5 Number of paths $N = 13$.

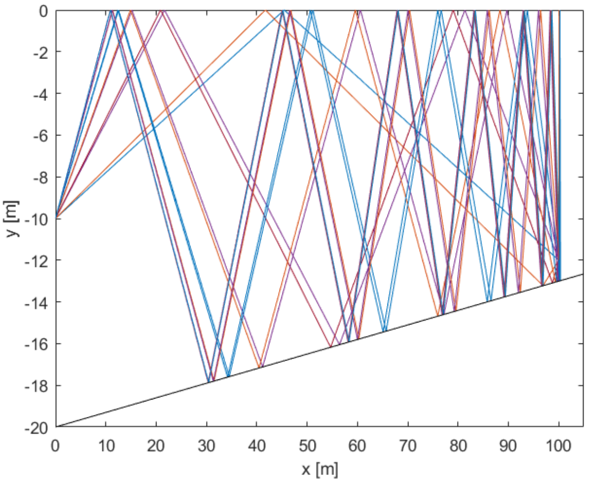

Fig. 7. Sound wave paths for a rising bottom slope angle $\beta = -4°$.

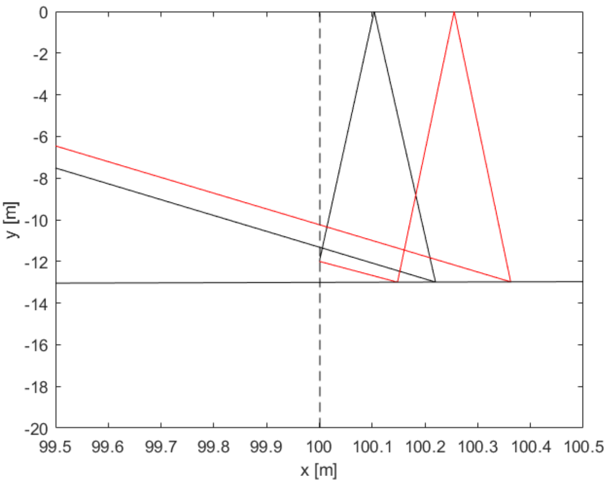

Fig. 8. Enlarged right section of Fig. 7. Number of paths $N = 14$.

In the enlarged sections of the paths, the reflection angles are apparently not equal to the incidence angles, which is due to the adoption of different scales of the X and Y axes. The path-setting program used features an incidence and reflection angle check and the results confirm the equality of all incidence and reflection angles.

An example of sound path-setting for the case of the first bottom reflection is shown in Fig. 9.

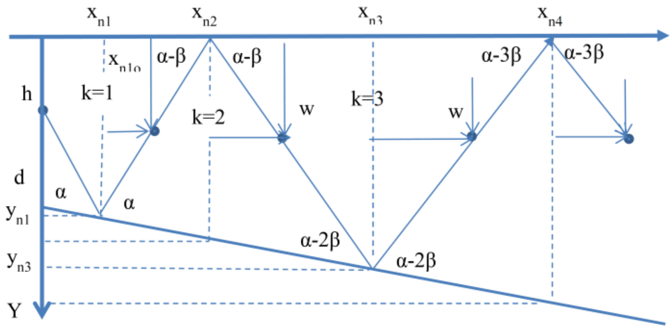

Fig. 9. Sound wave path when reflected first from the bottom.

Using the geometric regularities seen above, the coordinates x_{nk} and y_{nk} can be expressed with the Equations (11-20):

$$x_{n1} = \frac{d-h}{tg(\alpha_n+\beta)-tg\beta} \tag{11}$$

$$y_{n1} = d + x_{n1} tg\beta \tag{12}$$

- for odd reflections $k > 1$:

$$x_{nk} = \frac{d + x_{n(k-1)} tg[\alpha_n-(k-2)\beta]}{tg[\alpha_n-(k-2)\beta]-tg\beta} \tag{13}$$

$$x_{no} = \frac{d + x_{nk} tg\beta - w}{tg(\alpha_n - k\beta]} \tag{14}$$

$$y_{nk} = d + x_{n3} tg\beta \tag{15}$$

$$y_{no} = w \tag{16}$$

- for even reflections $k > 1$:

$$x_{nk} = \frac{d + x_{n(k-1)}\{tg[\alpha_n-(k-1)\beta]+tg\beta\}}{tg[\alpha_n-(k-1)\beta]-tg\beta} \tag{17}$$

$$x_{no} = \frac{w}{tg[\alpha_n-(k-1)\beta]} \tag{18}$$

$$y_{nk} = 0 \tag{19}$$

$$y_{nko} = w \tag{20}$$

To determine the angle α_n, Eq. (8) is solved numerically by inserting the above relations.

Fig. 10-12 show examples of sound wave path-setting for the channel parameters at which Fig. 2-4 were made.

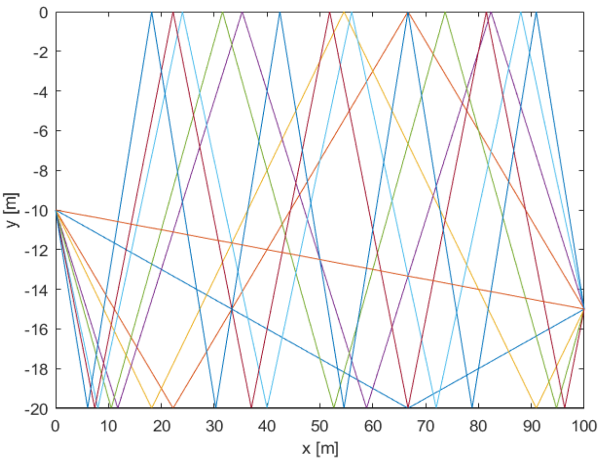

Fig. 10. Sound wave paths for a bottom slope angle β = 0°.

Analogous to the first reflection from the water surface, with larger bottom slope angles and more paths considered, there is a backward propagation.

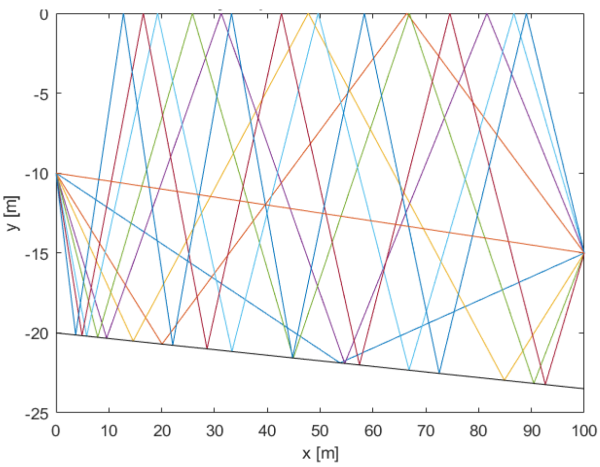

Fig. 11. Sound wave paths for a falling bottom slope angle β = 2°.

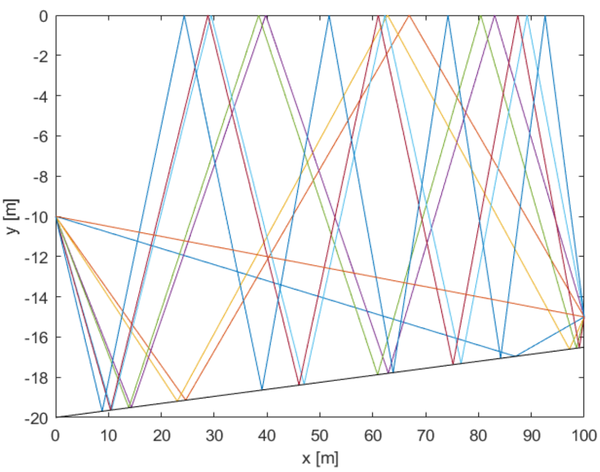

Fig. 12. Sound wave paths for a rising bottom slope angle β = −2°.

III. Pulse Responses and Transfer Functions

With the angles α_n determined and inserted into the relations given above, the coordinates of all the path sections are obtained. Their lengths are calculated from the Eq. (21):

$$r_{nk} = \sqrt{\left(x_{nk} - x_{n,k-1}\right)^2 + \left(y_{nk} - y_{n,k-1}\right)^2} \quad n = 2, \dots, N, k = 1, \dots, n \tag{21}$$

By summing the lengths expressed with the above formula, the wavelengths of the path for each number of reflections n is obtained from the Eq. (22):

$$s_n = \sum_{k=1}^{n} r_{nk} \tag{22}$$

Using these distances, the amplitudes of the received reflections are calculated assuming spherical propagation and absorption attenuation α_a is described by the Eq. (23):

$$A_n = \frac{s_1}{s_n} 10^{-\frac{\alpha_a s_n}{20}} A \tag{23}$$

where s_1 = 1 m, α_a is the logarithmic absorption attenuation coefficient in water [dB/m] and A is the amplitude of the pressure emitted by the transmitter at a distance s_1 from the surface. In the calculation results presented next, it is assumed that A = 1 and its physical size is ignored. Due to the low frequency of the transmitted signals and the small distances s_n, the effect of absorption attenuation, which is of the order of 1 dB/km, is also ignored.

The wave amplitudes are considerably reduced as a result of incomplete reflection from the water/bottom interface. The pressure reflection coefficient at this interface is described by the Eq. (24):

$$R_{nk} = \frac{z_d \sin \alpha_{nk} - z_w sin\beta_{nk}}{z_d \sin \alpha_{nk} + z_w sin\beta_{nk}} \tag{24}$$

where: α_{nk} is the angle of incidence at the bottom at reflection number n,k and β_{nk} is the angle of refraction at the water/bottom interface.[1)]

The incidence angles were determined numerically from the x_{nk} and y_{nk} coordinates expressed with the formulas above. The characteristic impedance of the bottom is denoted as z_d, while the same for water is denoted as z_w. A simplified assumption is made that the reflection coefficient at the water/air interface is $\alpha_{nk} = -1$.

The angle β_{nk} is determined from Snell's law:

$$\frac{cos\alpha_{nk}}{cos\beta_{nk}} = \frac{c_w}{c_d} \tag{25}$$

where: c_w is the sound wave velocity in the water, and c_d is the sound wave velocity within the bottom.

The delay of successive pulse responses is determined by the Eq. (26):

$$\tau_n = \frac{1}{c_w} s_n \tag{26}$$

[1)] In the literature, cosine angles are in the formula as they refer to the angles of incidence and refraction relative to the perpendicular from the reflecting surface. In this work, these angles relative to the reflecting surface are assumed, for graphical representation.

The pulse response $k(t)$ for the N sound wave paths considered is described by Eq. (27):

$$k(t) = \sum_{n=1}^{N} \left[A_n \left(\prod_{k=1}^{n} R_{n,k} \right) \delta(t - \tau_n) \right]_n \tag{27}$$

Fig. 13-15 show impulse responses, which are the totals of the responses for the sound wave paths at first reflection from the water surface (blue) and first reflection from the bottom (black). Red is the pulse arriving directly from the transmitter to the receiver. Impulse responses refer to the sound wave paths shown in the figures with the numbers given in the figure legends. Bottom reflection coefficients were determined for the sound velocity in water c_w = 1,500 m/s, and the sound velocity in the bottom sediment c_d = 1,800 m/s. The volume density of water is ρ_w = 1,000 kg/m^3 and the volume density of the bottom sediment was ρ_d = 3,000 kg/m^3. The specific sound impedances in Eq. (21) are $z_w = c_{w} \cdot \rho_w$ and $z_d = c_{d} \cdot \rho_d$.

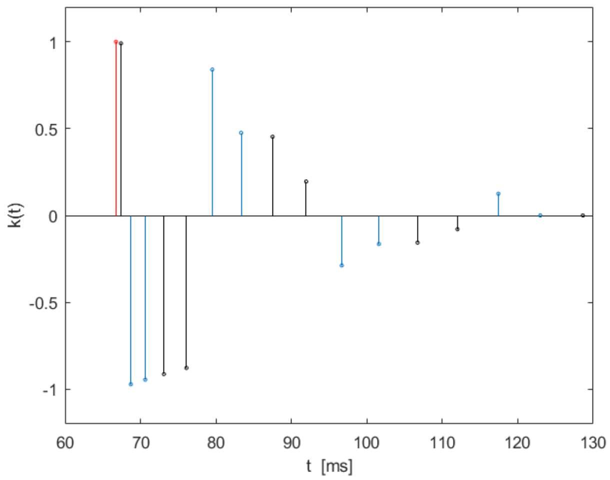

Fig. 13. Impulse response for a bottom slope β = 0° (sound wave paths in Fig. 2 and Fig. 10).

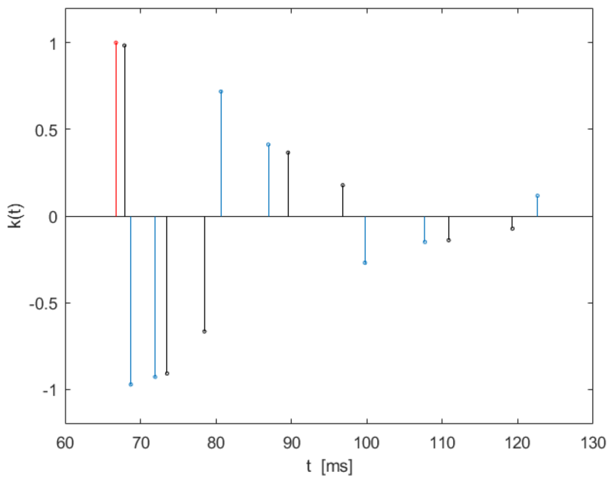

Fig. 14. Impulse response for a bottom slope β = 2° (sound wave paths in Fig. 3 and Fig. 11).

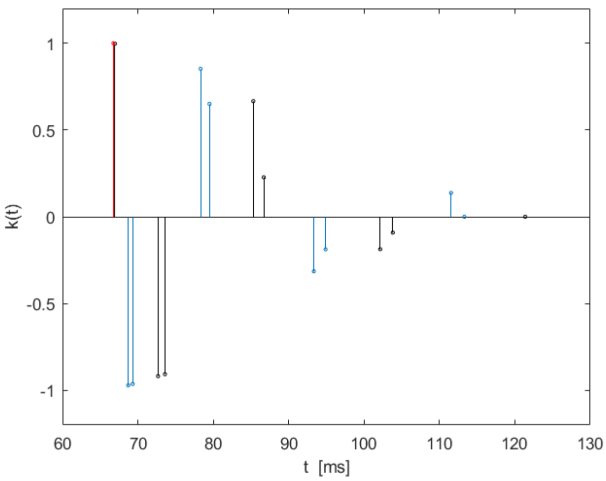

Fig. 15. Impulse response for a rising bottom slope β = −2° (sound wave paths in Fig. 4 and Fig. 12).

Impulse responses at different bottom slope angles vary mainly in the time distribution of the Dirac pulse position. This results in the large differences in the transfer function shown in the Fig. 16-18

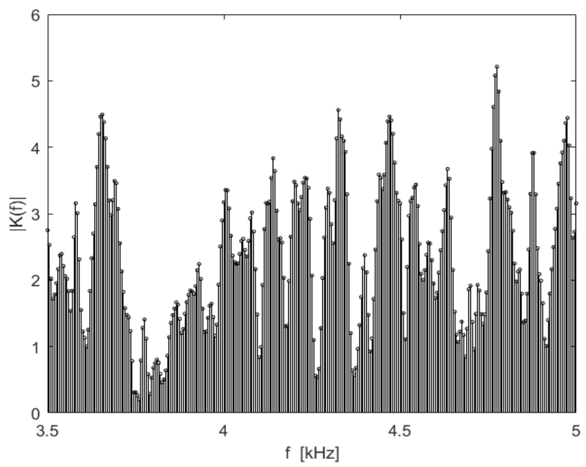

Fig. 16. Transfer function for a bottom slope β = 0° (impulse response in Fig. 13).

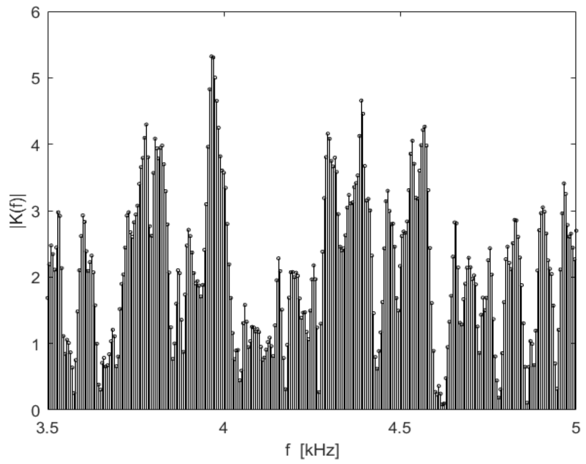

Fig. 17. Transfer function for a bottom slope β = 2° (impulse response in Fig. 14).

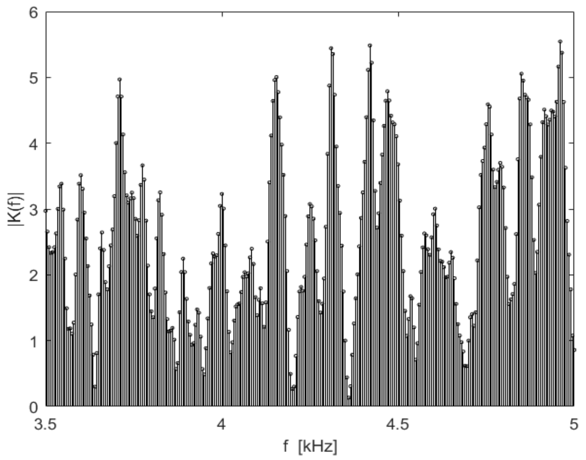

Fig. 18. Transfer function for a bottom slope $\beta = -2°$ (impulse response in Fig. 15).

IV. SIGNAL TRANSMISSION

The analysis of impulse responses and transfer functions does not provide clear answers as to the effect of the bottom slope on the transmission of sound signals in the system discussed here. Due to significant fading of transfer functions it is clear that the quality of transmission is in any case dependent on the choice of carrier frequency. The narrower the spectral width of the transmitted signals, the greater the relationship.

The system discussed here is intended to have the capability to transmit signals also to objects buried in the bottom, which requires the use of low frequencies [1]. Hence, the transmission examples presented below will be limited to such frequencies. The purpose of the system to transmit digital information implies the need for pulsed signals. We will therefore consider the transmission of narrowband pulses with a rectangular envelope and broadband pulses with a linear frequency modulation.

Signal processing at the receiver starts with the determination of the received signal. The received signal $x(t)$ is the result of the convolution of the transmitted signal $s(t)$ and the pulse response $k(t)$:

$$x(t) = k(t) * s(t) \tag{28}$$

Gaussian noise with standard deviation σ is added to the received signal. The Gaussian noise is determined from the assumed SNR_i [1].

For narrowband pulses, the sum of signal and noise is processed by narrowband filters with middle frequencies equal to the carrier frequencies of the transmitted pulses. The bandwidth of the filters is equal to:

$$B = \frac{1}{\tau} + \frac{v_{max}}{c} f_0 \tag{29}$$

where τ is the pulse duration, v_{max} is the maximum velocity of the transmitter, c is the sound wave velocity, and f_0 is the pulse carrier frequency.

Eighth-order Butterworth filters were used in the simulation program. After filtering, envelope detection is performed by rectifying the signal and passing it through lowpass Butterworth filter with bandwidth equal to B.

In the case of frequency-modulated signals, matched filtering was used, as described by the relationship in Eq. (30):

$$z(t) = \mathcal{F}^{-1}\{\mathcal{F}\{k(t)\} \cdot \mathcal{F}^{*}\{x(t) + n(t)\}\} \tag{30}$$

where $\mathcal{F}$ denotes the Fourier transform and $*$ is the conjugation operator.

After matched filtering, envelope detection is applied, such as for narrowband pulses. To illustrate the transmission of narrow-band sinusoidal pulses, two pulses were used with carrier frequencies f_0 = 4 kHz and f_1 = 4.7 kHz, duration τ = 2.5 ms at intervals of 5τ = 12.5 ms. They represent the ‘0’ and ‘1’ bits. The transmitter is stationary and the filter bandwidth is B = 500 Hz. Fig.19-22 show the baseband envelopes of output signals for the channels whose impulse responses are shown in Fig. 13-15 respectively.

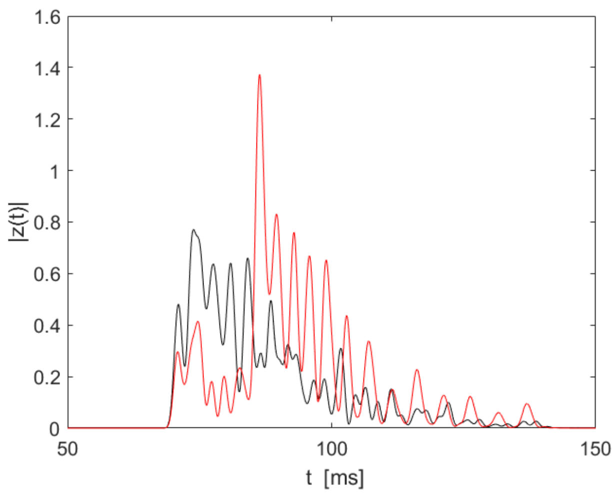

Fig. 19. Baseband envelope of output signal for a bottom slope $\beta = 0°$ (impulse response in Fig. 13).

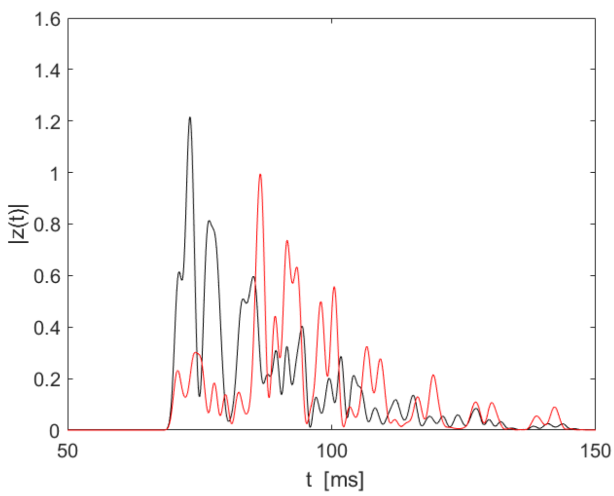

Fig. 20. Baseband envelope of output signal for a bottom slope $\beta = 2°$ (impulse response in Fig. 14).

With very short pulses, the output signal largely reproduces the impulse response waveform. The effect of the bottom slope angle affects the ratio of pulse heights representing the bits. However, this is not a constant trend, as the ratios depend mainly on the choice of carrier frequencies. This is illustrated in Fig. 22, for which the frequency f_1 = 4.5 kHz was changed and v = 10 m/s was assumed.

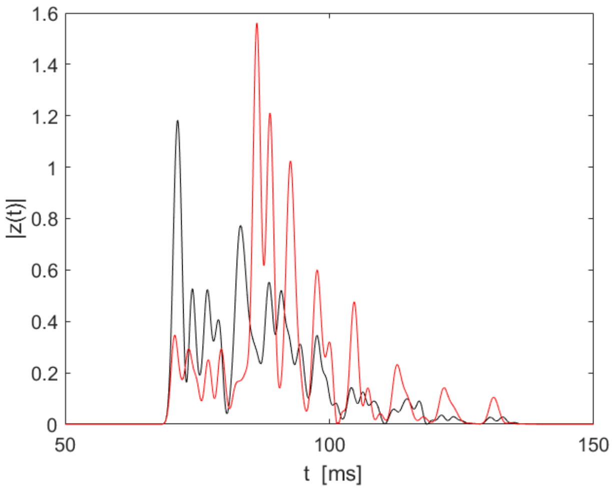

Fig. 21. Baseband envelope of output signal for a bottom bottom slope $\beta = 0°$ (impulse response in Fig. 13).

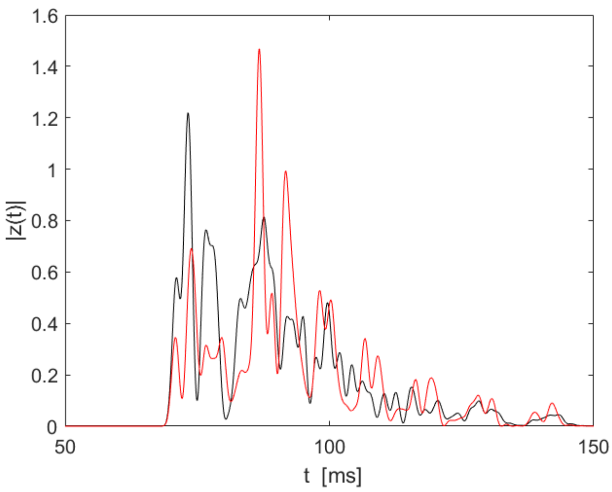

Fig. 22. Baseband envelope of output signal for a bottom bottom slope $\beta = 2°$ (pulse response in Fig. 14).

Random differences in signal heights prevent using threshold detection in the reconstruction of the transmitted bit sequence. It can be reproduced by comparing the maximum values of signals of different frequencies in successive transmission intervals, as was done in the following calculations. If the maximum in the carrier frequency band f_0 is greater in the time interval corresponding to bit ‘0’, the transmission is error-free. Otherwise, an error occurs. Error probabilities were measured using the example of a pair of pulses with carrier frequencies f_0 = 4 kHz and f_1 = 4.7 kHz with duration τ = 2.5 ms. The pulse interval is 50 ms and equal to the assumed pulse response duration. Calculations were performed for three different bottom slope angles β, varying the spectral power density of noise N. The number of samples is 10,000 and the result is shown in Fig. 23. Positive bottom slope angles result in an increase in the error rate, while negative angles decrease the number of errors. This trend is corroborated by other completed transmission examples. Interestingly, it is not noticeably influenced by input signal-to-noise ratios SNR_i, asits increase does not always result in a decrease in errors. An error rate of less than 1 per 10,000 samples is achieved on average by the transmission system discussed here at SNR_i > 20 dB.

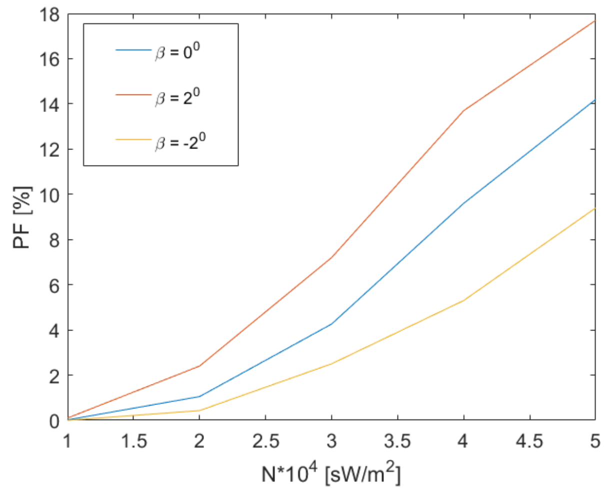

Fig. 23. Average error rate per bit transmitted.

In this transmission example, the transmission rate is approximately 200 bps, which is relatively high. A reduction in the required SNR_i can be achieved at the expense of a reduction in the transmission rate by using pulses with linear frequency modulation, LFM.

Fig. 26 shows the transmission simulation results of a pair of LFM pulses (Fig. 24-25) with middle frequencies f_0 = 4 kHz and f_1 = 4.7 kHz, bandwidth B equal to 0.4 kHz and duration τ equal to 0.5 s. The second pulse is delayed by 0.1 s. The transmission is in a channel such as for narrowband pulses. The matched filtration described by formula (27) was used.

The result of matched filtering is time compression of the transmitted signals.

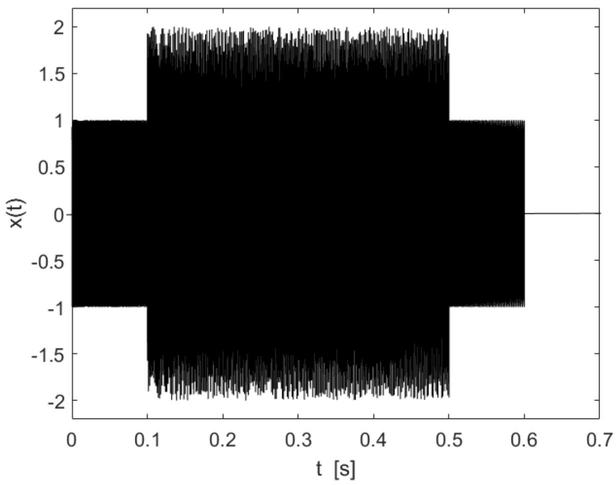

Fig. 24. Signal transmitted.

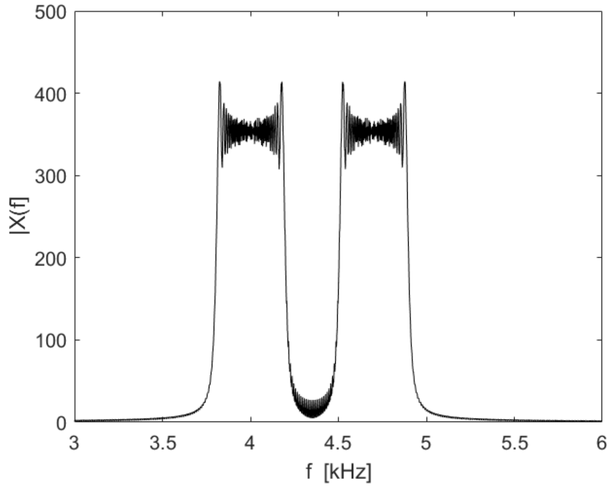

Fig. 25. Transmitted signal spectrum.

The output signals after matching filtering are presented in Fig. 27 for slope angel β = 2°, in Fig. 28 for slope angel β = 0° and in Fig. 29 for slope angel β = -2°.

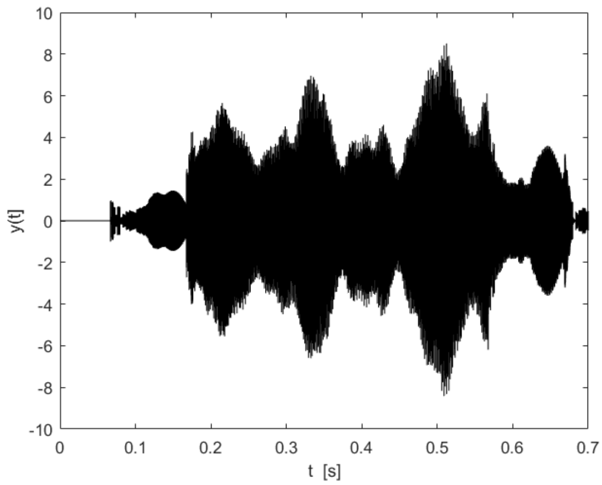

Fig. 26. Received signal.

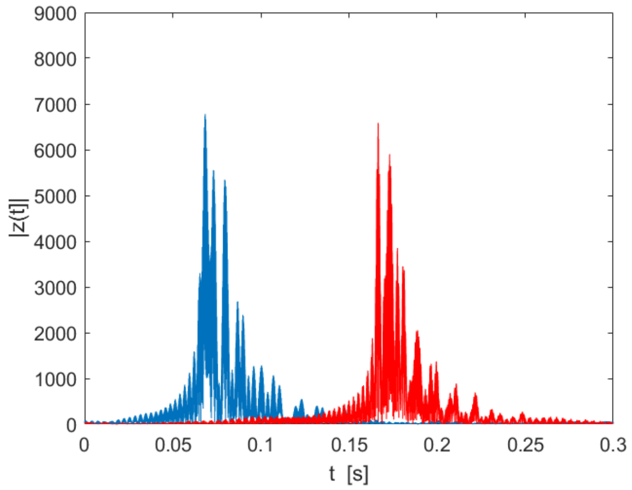

Fig. 27. Signals after matched filtering; β = 2°.

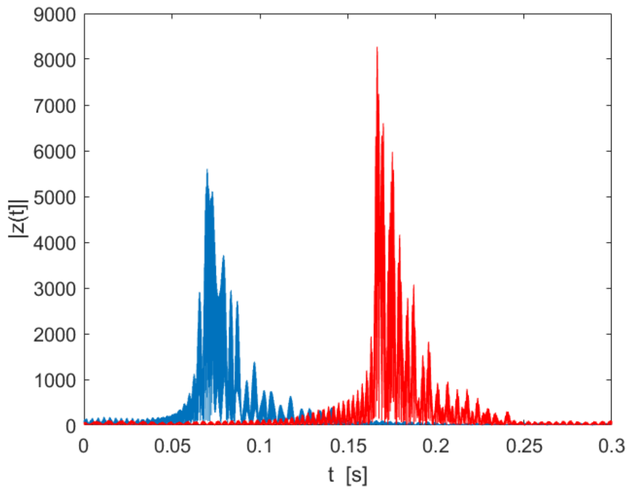

Fig. 28. Signals after matched filtering; β = 0°.

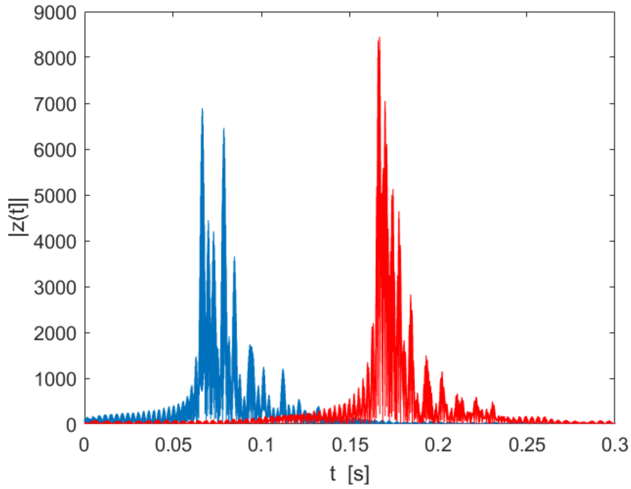

Fig. 29. Signals after matched filtering; $\beta = -2°$.

As with narrowband pulses, there are differences in signal heights from different carrier frequencies and different bottom slope angles β. To investigate the impact of this slope, transmission error calculations were performed, as discussed above. The calculation results are shown in Fig. 30.

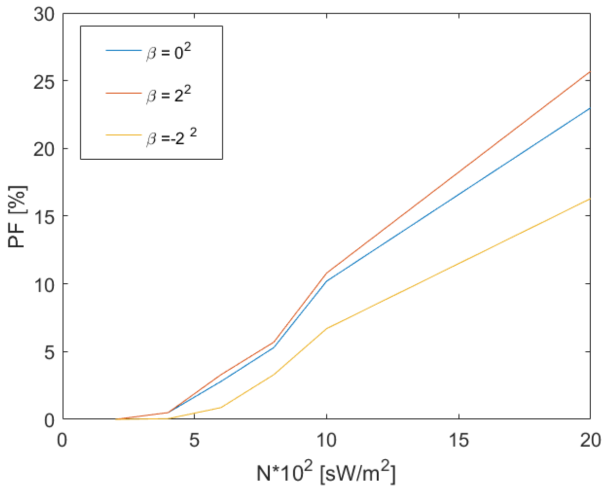

Fig. 30. Average error rate per bit transmitted.

There is a noticeable trend, as noted earlier, of the error rate decreasing when the bottom slope angle is negative. Compared to a transmission using narrowband pulses, correct transmission occurs with a significantly lower input SNR. Less than one error per 10.000 samples is achieved at approximately SNR_i = 5.8 dB for $\beta = 0°$ and $\beta = 2°$ and SNR_i = 4.9 dB, which is approximately 14 dB less than for the transmission of narrowband pulses. With full matching [$k(t) = \delta(t)$], the improvement should be $10\log(B \cdot \tau) = 10\log(200) = 23$ dB. The negative impact of multi-path transmission on the detection of transmitted signals is apparent.

The transmission rate of LFM signals is lower than that of narrowband pulses, but does not increase in proportion to the duration of the pulses, and the disproportion is smaller the longer the bit string transmitted. In the examples considered here, it takes 0.3 s to transmit a five-bit word when transmitting narrowband pulses, and 0.9 s for LFM signals. Despite the 200-fold increase in pulse length, the transmission time has only increased threefold.

Conclusion

- Bottom slope angles more than 0 (falling slope) worsen the transmission conditions.
- Bottom slope angles less than 0 (rising slope) improve the transmission conditions.
- This trend occurs for narrowband pulses and LFM pulses
- Better transmission conditions exist for LFM signals regardless of the bottom slope angle.

Notice

In the paper – "Part B", these authors demonstrate the effect of bottom slope on transmission with the receiver buried in the bottom sediment.

References

[1] R. Salamon, J. Marszal, I. Kochańska., "Shallow Water Communication with an Object Buried in Bottom Sediments", Intl Journal of Electronics and Telecommunications, 2024, Vol. 70, No. 4, pp. 805-813. doi:10.24425/ijet.2024.152064

[2] I. Kochańska, A. M. Schmidt, JH. Schmidt, "Shallow-Water Acoustic Communications in Strong Multipath Propagation Conditions", *2024 14th International Symposium on Communication Systems, Networks and Digital Signal Processing (CSNDSP),* IEEE *Xplore,* pp. 99-103, 2024. doi: 10.1109/CSNDSP60683.2024.10636410

[3] J. H. Schmidt, A. M. Schmidt, I. Kochańska, R. Studański, A. Żak, "Performance of underwater data transmission using incoherent modulation MFSK in very shallow waters", *International Journal of Electronics and Telecommunications,* vol. 70, no.4, pp. 861-869, 2024. doi: 10.24425/ijet.2024.152071

[4] J. H. Schmidt, I. Kochańska, A. M. Schmidt,"Performance of the Direct Sequence Spread Spectrum Underwater Acoustic Communication System with Differential Detection in Strong Multipath Propagation Conditions", *Archives of Acoustics,* vol. 49, no. 1, pp. 129-140. doi: 10.24425/aoa.2024.148771

[5] J. Schmidt, I. Kochańska, A. Schmidt, "Measurement of impulse response of shallow water communication channel by correlation method", *Hydroacoustics*, vol. 20, pp. 149-158, 2017.

[6] I. Kochańska, J. H. Schmidt, J. Marszal, "Shallow water experiment of OFDM underwater acoustic communications", *Archives of Acoustics*, vol. 45, no. 1, 11-18, 2020, doi: 10.24425/aoa.2019.129737

[7] J. B. Allen, D. A. Berkley, "Image method for efficiently simulating small-room acoustics". *J. Acoust. Soc. Am.*, vol. 65, no. 4, pp. 943-950, 1979. doi: 10.1121/1.382599

[8] A. Wareing, M. Hodgson, "Beam-tracing model for predicting sound fields in rooms with multilayer bounding surfaces, *J. Acoust. Soc. Am.*, vol. 118, no. 4, pp. 2321-2331, 2005. doi: 10.1121/1.2011152

[9] G. Marbjerg, J. Brunskog, C. H. Jeong, E. Nilsson, "Development and validation of a combined phased acoustical radiosity and image source model for predicting sound fields in rooms". *J. Acoust. Soc. Am.*, vol. 138, no.3, pp. 1457-1468, 2015. doi:10.1121/1.4928297

[10] M. Stojanovic, J. Preisig, "Underwater acoustic communication channels: prpagation models and statistical characterisation", *IEEE Communications Magazine*, January 2009, pp. 84-89, 2009. doi: 10.1109/MCOM.2009.4752682

[11] T. C. Yang, "Properties of underwater acoustic communication channels in shallow water", *J. Acoust. Soc. Am.*, vol. 131, no. 1, pp. 129-145, 2012. doi: 10.1121/1.3664053

[12] P. A. van Walree, "Propagation and scattering effects in underwater acoustic communication channels", *IEEE J. Ocean Eng.*, vol. 38, no. 4, pp. 614-631, 2013.

[13] F. John, M. Cimdins, H. Hellbrück, "Underwater ultrasonic multipath diffraction model for short range communication and sensing applications", *IEEE Sensors Journal*, vol. 21, no. 20, pp. 22934-22943, 2021.